Supporting Information

O-vacancy and PANI dual modifying titanium dioxide for fast sodium storage

Wen-Hua Shi, [a] Zhi-Wen Yin, [a, b] Jing Liu, [a] Zhi-Yi Hu, [a, b] Hemdan S. H. Mohamed [c], Li-Hua Chen, [a] Yu Li *[a] and Bao-Lian Su *[a, d]

[a] State Key Laboratory of Advanced Technology for Materials Synthesis and Processing, Wuhan University of Technology, Wuhan 430070, Hubei, China

[b] Nanostructure Research Centre (NRC), Wuhan University of Technology, Wuhan 430070, Hubei, China

[c] Physics Department, Faculty of Science, Fayoum University, El Gomhoria Street, 63514 Fayoum, Egypt.

[d] Laboratory of In-organic Materials Chemistry (CMI), University of Namur, B-5000 Namur, Belgium

*Corresponding author. yu.li@whut.edu.cn (Y. Li) and bao-lian.su@unamur.be (B. L. Su)

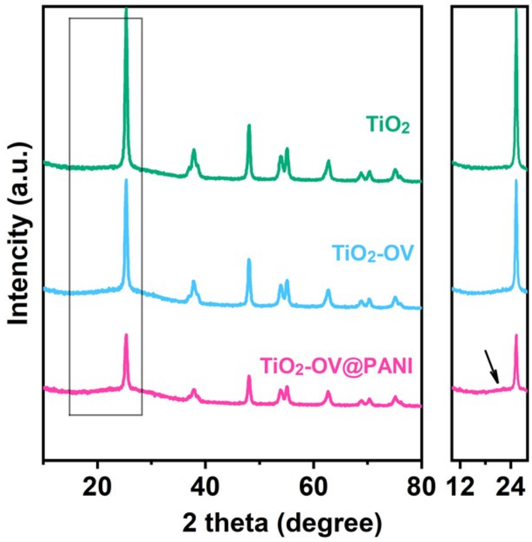

Figure S1. XRD patterns of TiO_2, TiO_2-OV and TiO_2-OV@PANI.

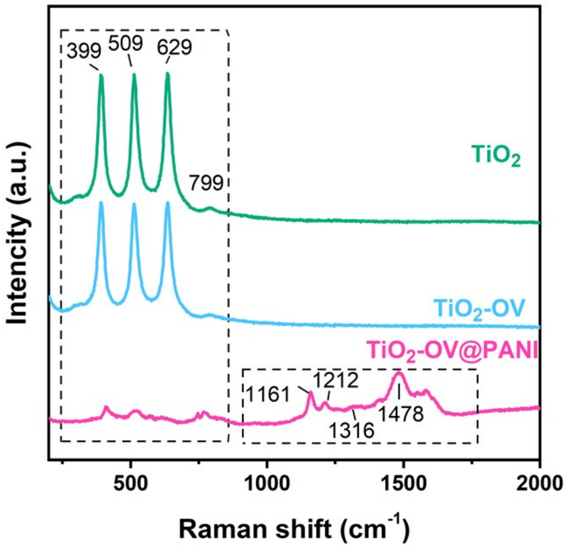

Figure S2. Raman spectra of TiO_2, TiO_2-OV and TiO_2-OV@PANI.

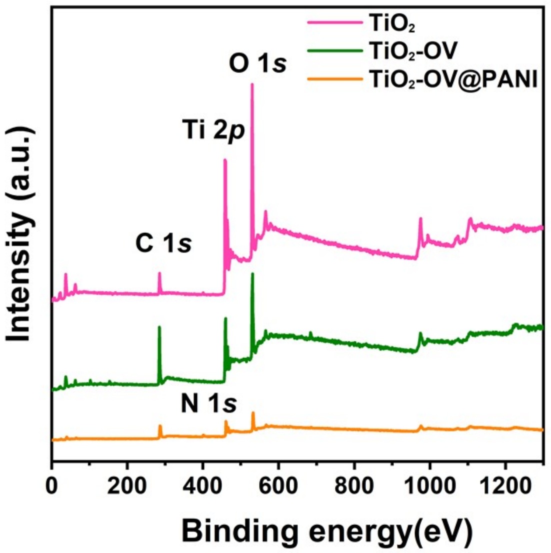

Figure S3. Survey XPS spectrum of TiO_2, TiO_2-OV and TiO_2-OV@PANI.

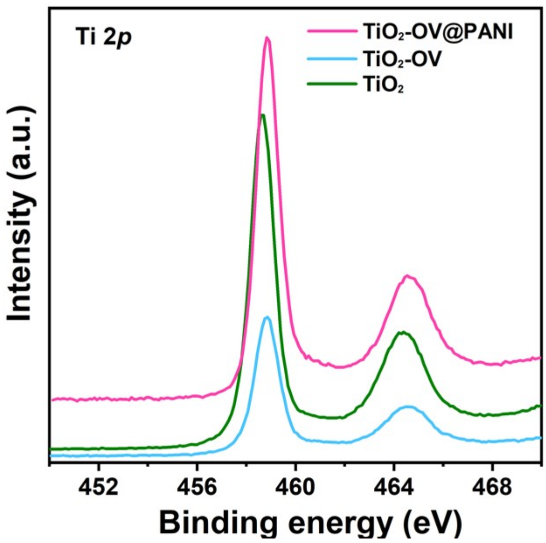

Figure S4. The high-solution Ti 2*p* XPS spectra of TiO_2, TiO_2-OV and Ti-OV@PANI

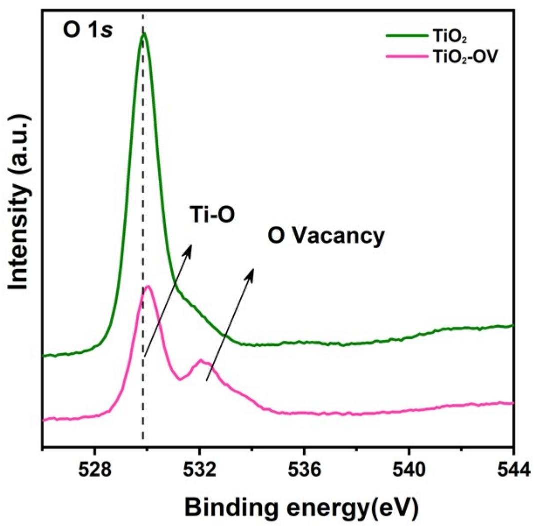

Figure S5. The high-solution O 1*s* XPS spectra of TiO_2, TiO_2-OV.

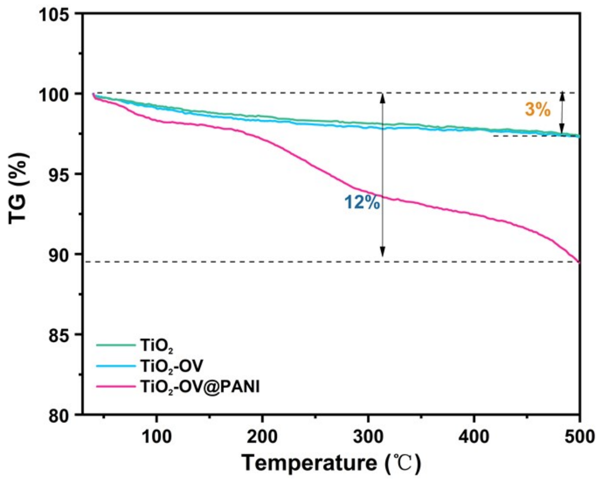

Figure S6. The TG curves of TiO_2, TiO_2-OV and TiO_2-OV@PANI.

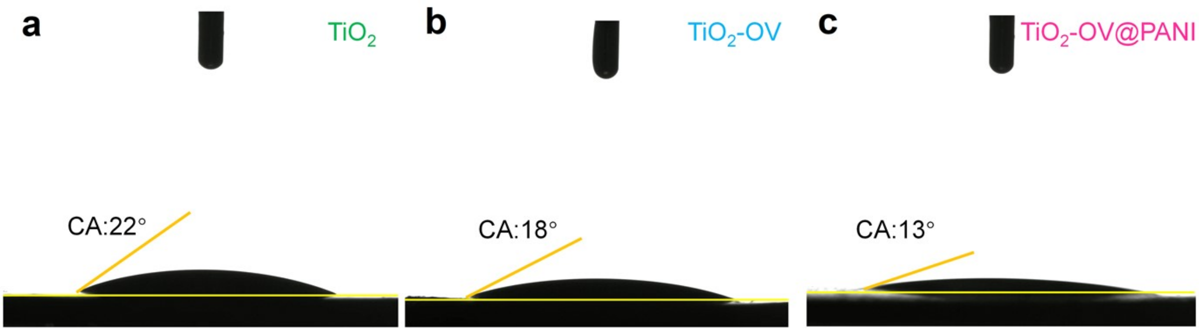

Figure S7. The contact angles of TiO_2, TiO_2-OV and TiO_2-OV@PANI.

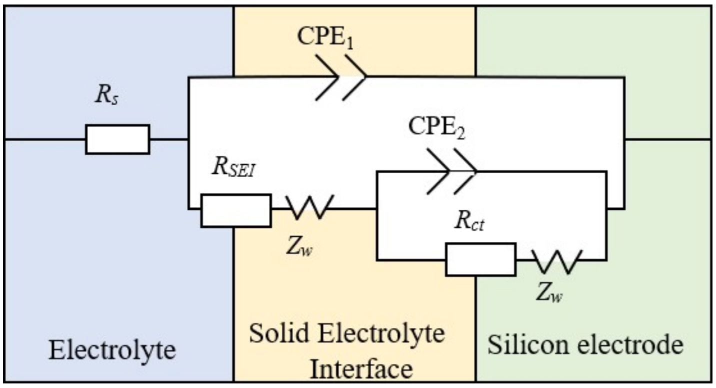

Figure S8. EIS impedance fitting element diagram.

The details of the EIS analysis for the diffusion coefficients of Na^+ (D_{Na^+})

The EIS spectra have a long diagonal line in the low-frequency region, which is mainly controlled by diffusion. **Formula 1** shows a relationship curve between the Z' and $\omega^{-1/2}$. According to the formula below (**Formula 2)**, the following is the formula for calculating the lithium-ion diffusion coefficient[1].

$$Z'=R_s+R_{ct}+\sigma\omega^{-1/2} \qquad \textbf{Formula 1}$$

$$D_{Na^+}=R^2T^2/2A^2n^2F^4C^2\sigma^2 \qquad \textbf{Formula 2}$$

In the formula, Z' is the total real resistance and ω is the angular frequency, R is the gas constant, T is the absolute temperature, A is the effective area of the electrode material, n is the number of electrons transferred, C is the lithium concentration in the electrode, and σ is the Warburg coefficient.

The details of the pseudocapacitive contribution of electrode material

Pseudo-capacitance, alternatively referred to as Faraday quasi-capacitance, is a phenomenon based on ion absorption and detachment, which accurately reflects the characteristics of the electrode material. The contribution of pseudo-capacitance can be computed using the formula presented below. **(Formula S3)**

$$i = av^b \qquad \textbf{Formula S3}$$

In **Formula S3**, '*i*' represents the current, and '*v*' stands for the potential scan rate [2, 3]. By analyzing cyclic voltammetry (CV) curves at various scan rates, the 'b' value can be derived through a fitting calculation based on **Formula S3**. A '*b*' value of less than or equal to 0.5 indicates diffusive properties of the electrode material. When '*b*' lies between 0.5 and 1, it suggests the presence of both diffusive and pseudo-capacitance properties in the electrode material. A '*b*' value greater than or equal to 1 signifies the dominance of pseudo-capacitance in the electrode material. When '*b*' falls between 0.5 and 1, the contribution rate of pseudo capacitance can be determined by dividing the area under the pseudo capacitance curve by the area under the original CV curve.

The details for First-principles computations

All density functional theory (DFT) calculations were conducted using the Vienna Ab initio Simulation Package (VASP) [4, 5]. The exchange-correlation potential was treated with the Perdew−Burke−Ernzerhof (PBE) generalized gradient approach (GGA)[6]. Electron-ion interactions were described by the projector augmented wave (PAW) method [7]. A cutoff energy of 400 eV was employed for the plane-wave basis set. The Brillouin zone was sampled using a 3 × 3 × 3 k-point grid for TiO_2 and TiO_2-OV, while a 1 × 1 × 1 grid centered at the Γ point was used for TiO_2-OV-PANI due to its large slab size. The convergence criteria for self-consistent iterations were set to 10^{-5} eV for total energy and 0.02 eVÅ^{-1} for force. Additionally, a DFT+U correction was applied to the Ti atoms with a U-J value of 3.0. Van der Waals (VdW) interactions were accounted for using the DFT-D3 method[8]. Visualization of the results was performed using VESTA software. The Na adsorption energies (E_{ads}) were calculated according to the following **Formula 4**

$$E_{ads} = E_{*2Na}–2E_{Na}–E_{Sub} \qquad \textbf{Formula 4}$$

where E_{*2Na} is the total energy of the system with two Na atoms adsorbed on the substrate, E_{Sub} is the energy of the clean surface, and E_{Na} is the energy of a single Na atom.

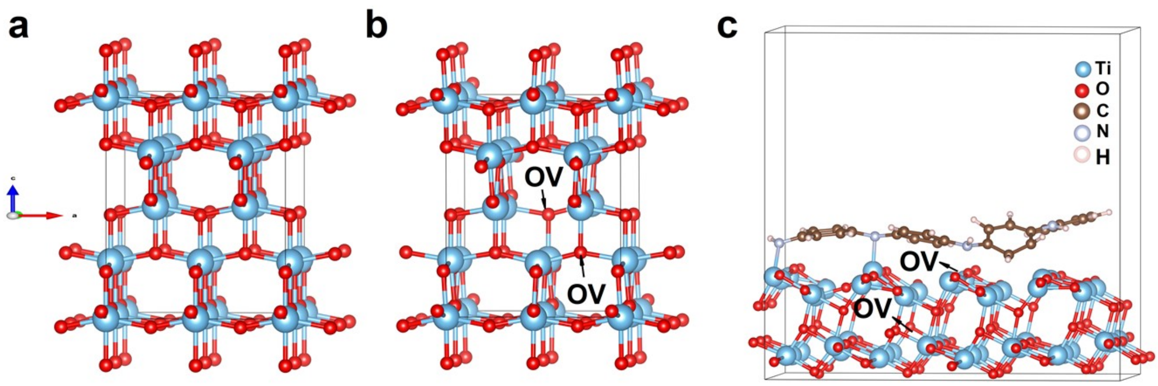

Figure S9. The models of TiO_2, TiO_2-OV and Ti-OV-PANI.

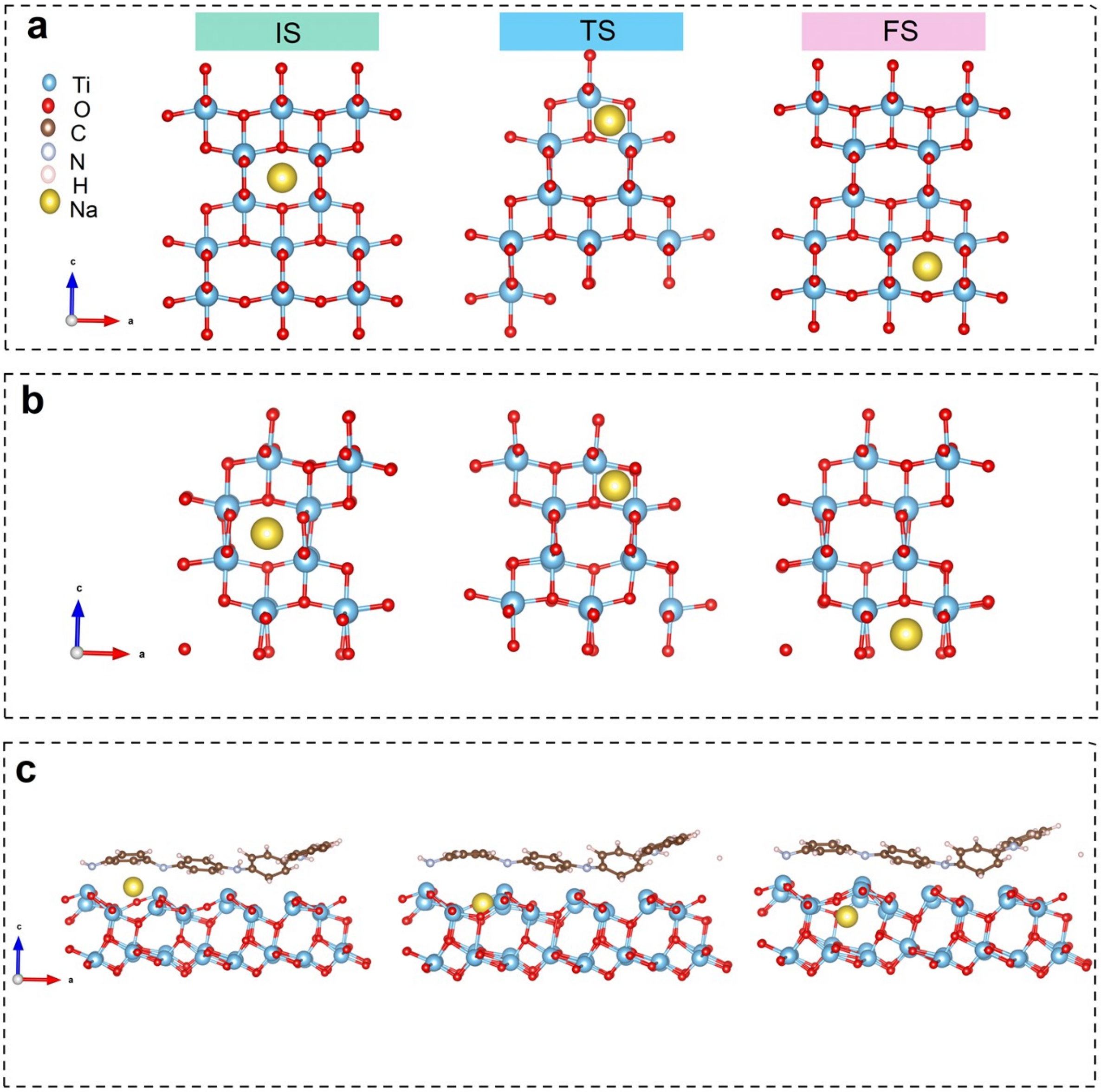

Figure S10. The Na^+ migration paths in (a) TiO_2, (b) TiO_2-OV and (c) TiO_2-OV-PANI.

Table S1 The comparison of the performance of our TiO_2 anode with previous reported TiO_2-based anodes for Na storage.

Materials	Rate performance		References
	Capacity	Current density	
N-dopedTiO_2/ MXenes	0.1	250	9
	0.2	196	
	0.5	157	
	1	129	
TiO_2/CNTs	0.1	250	10
	0.2	231	
	1.5	167	
	3	143	
TiO_2@$TiOF_2$	0.1	211	11
	0.2	198	
	0.5	165	
	1	151	
	2	137	
TiO_2 NWs/RGO	0.05	250	12
	0.2	187	
	0.5	162	
	2	144	
SL-mTiO_2	0.5	179	13
	1	160	
	2	142	
TiO_2-Bi/CNFs	0.1	244	14
	0.2	216	
	0.5	171	
	1	131	
	2	93	
N-TiO_2-NTs	0.07	210	15
	0.34	154	
	1.7	125	
	3.4	114	
TiO_2-OV@PANI	0.1	220	This work
	0.2	197	
	0.5	183	
	1	165	
	2.5	144	

References

1. Y. Zhu, Y. Xu, Y. Liu, C. Luo and C. Wang, Comparison of electrochemical performances of olivine $NaFePO_4$ in sodium-ion batteries and olivine $LiFePO_4$ in lithium-ion batteries, *Nanoscale*, 2013, **5**, 780-787.
2. M. Yin, X. Feng, D. Zhao, Y. Zhao, H. Li, W. Zhou, H. Liu, X. Bai, H. Wang, C. Feng and Q. Jiao, Hierarchical Co_9S_8@carbon hollow microspheres as an anode for sodium ion batteries with ultralong cycling stability, *ACS Sustain. Chem. Eng.*, 2019, **7**, 6122-6130.
3. J. Liu, J. Wang, C. Xu, H. Jiang, C. Li, L. Zhang, J. Lin and Z. X. Shen, Advanced energy storage devices: Basic principles, analytical methods, and rational materials design, *Adv. Sci.*, 2018, **5**, 1700322.
4. G. Kresse and J. Hafner, Ab initio molecular dynamics for liquid metals, *Phys. Rev. B* 1993, **47**, 558-561.
5. G. Kresse and J. Hafner, Ab initio molecular-dynamics simulation of the liquid-metal--amorphous-semiconductor transition in germanium, *Phys. Rev. B* 1994, **49**, 14251-14269.
6. L. B. Hansen and J. K. Nørskov, Improved adsorption energetics within density-functional theory using revised Perdew-Burke-Ernzerhof functionals, *Phys. Rev. B* 1999, **59**, 7421.
7. J. P. Perdew, K. Burke and M. Ernzerhof, Generalized gradient approximation made simple, *Phys. Rev. Lett.*, 1996, **77**, 3865-3868.
8. S. Grimme, J. Antony, S. Ehrlich and H. Krieg, A consistent and accurate ab initio parametrization of density functional dispersion correction (DFT-D) for the 94 elements H-Pu, *J. Chem. Phys.*, 2010, **132**, 154104.
9. X. Y. Wang, Q. H. Yang, K. Li and M. M. Zhen, Defects introducing and heterostructures engineering synergistically constructing active sites for achieving stable and fast ion transport in sodium-ion batteries, *J. Alloy Compd.*, 2024, **1003**, 175676.
10. W.-B. Yu, W.-D. Dong, C.-F. Li, N. Macadam, J.-X. Yang, G.-B. Zhang, Z.-Y. Hu, T.-C. Wu, Y. Li, T. Hasan, L.-H. Chen, L.-Q. Mai and B.-L. Su, Interwoven scaffolded porous

titanium oxide nanocubes/carbon nanotubes framework for high-performance sodium-ion battery, *J. Energy Chem.*, 2021, **59**, 38-46.

11. S. Guan, Q. Fan, Z. Shen, Y. Zhao, Y. Sun and Z. Shi, Heterojunction TiO_2@$TiOF_2$ nanosheets as superior anode materials for sodium-ion batteries, *J. Mater. Chem. A*, 2021, **9**, 5720-5729.
12. J. G. Yu, H. Huang, Y. P. Gan, Y. Xia, C. Liang, J. Zhang, X. Y. Tao and W. K. Zhang, A new strategy for the construction of 3D TiO_2 nanowires/reduced graphene oxide for high-performance lithium/sodium batteries, *J. Mater. Chem. A*, 2018, **6**, 24256-24266.
13. K. Lan, Y. Xia, R. C. Wang, Z. W. Zhao, W. Zhang, X. M. Zhang, A. Elzatahry and D. Y. Zhao, Confined interfacial monomicelle assembly for precisely controlled coating of single-layered titania mesopores, *Matter*, 2019, **1**, 527-538.
14. S. N. Liu, X. X. Chen, M. Y. Li, X. C. Zhang, Y. Y. Sun, J. Yang, W. Li and Z. Y. Cai, Electrospun Bi-doped TiO_2/C nanofibers as active materials for high- capacity and long-life-stability sodium-ion anodes, *J Electroanal Chem*, 2022, **924**, 38-46.
15. Y. Qu, S. M. Zhu, X. F. Dong, H. Huang and M. Qi, Nitrogen-doped TiO_2 nanotube anode enabling improvement of electronic conductivity for fast and long-term sodium storage, *J. Alloy Compd.*, 2021, **889**, 161612.